Kinetic and Structural Model for the Binding of Formate to the Rapid Form of Cytochrome *c* Oxidase†

Gary M. Baker* and Stephen M. Gullo

Department of Chemistry, Northern Illinois University, De Kalb, Illinois 60115

Received February 18, 1994; Revised Manuscript Received May 10, 1994®

ABSTRACT: The binding of formate to the rapid form of cytochrome *c* oxidase from bovine heart has been examined at pH 8.8 and high ionic strength. The optical changes included (1) a transient decrease at 414 nm, followed by a biphasic increase, and (2) an isosbestic wavelength. The apparent blue shift in the Soret envelope, following the transient, was consistent with a 430 → 414 transition in cytochrome a_3, described previously for acid jump conditions in the absence of formate [Papadopoulos, P. G., Walter, S. A., Li, J., & Baker, G. M. (1991) *Biochemistry 30*, 840–850]. A two-step binding mechanism was implied by the biphasic increase, but the k_{obs} values for each phase, when plotted against formate concentration, were unable to statistically discriminate two rival kinetic models. Both models postulated a rapid 430 + L ⇌ 414·L step (where L = HCOOH + $HCOO^-$), but they differed in whether the slower step depended on L. The equilibrium dissociation constant, K_D^{app}, for the overall binding reaction was 0.3 mM. An analysis of the rival mechanisms indicated this value to be consistent with a step that was independent of L. A slow 414·L ⇌ 414′·L conversion was therefore postulated, and the K_{eq} for this step was found to be ≈9. The analysis to this point assumed that cytochrome a_3 was entirely in the 430 state at the time of formate addition. Modeling of the transient could not be achieved, however, unless cytochrome a_3 was present as a rapid equilibrium mixture of 414 and 430 states. The 414, 414·L, and 414′·L states were assumed to be electronically identical to account for the isosbestic wavelength. Numerical simulations of a four-state binding model provided a good fit at both 1 and 25 mM formate and further suggested that the 414′·L state may be the slow conformer that is detected by cyanide. A structural model consistent with these kinetic constraints is proposed.

Exogenous ligands that bind cytochrome *c* oxidase (ferrocytochrome *c*:O_2 oxidoreductase, EC 1.9.3.1) have been used by many investigators as probes of binulcear site structure. Most of those studies, which have been done with detergent-solubilized enzyme from bovine heart, have shown the a_3-(III)–Cu_B(II) site to be heterogeneous by both spectral and kinetic criteria. The use of cyanide and hydrogen peroxide, in particular, has led to extensive characterization of rapid and slow forms of cytochrome *c* oxidase (Baker et al., 1987; Palmer et al., 1988; Moody et al., 1991; Weng & Baker, 1991). The rapid form, which is stabilized at high pH (>8) and high heme *a* concentration (Baker et al., 1987; Gullo et al., 1993), shows k_{obs} values of 0.01–0.06 s^{-1} when reacted with saturating concentrations of these ligands. Acidic pH or extreme dilution of the enzyme, during or after purification, induces irreversible conversion to a slow form that shows 100–300-fold slower rates of binding (Baker et al., 1987; Gullo et al., 1993).

The evidence suggests that rapid and slow forms differ in their axial ligation, probably at the position that bridges the a_3 and Cu_B sites. In a recent magnetization study, Day et al. (1993) have shown that the rapid conformer has a large, positive zero field splitting parameter, *D*, that changes sign in the slow form. The negative *D* value implies a stronger interaction between the Fe(III) center and the putative bridge. The slow form is also characterized by an EPR signature at $g' = 12$ (Brudvig et al., 1981, 1986; Baker et al., 1987). A weaker signal at $g' = 2.95$ has been reported that exhibits the same power saturation and temperature dependence as $g' = 12$ (Cooper & Salerno, 1992). Both features are absent in the rapid form. Day et al. (1993) have also suggested that rapid enzyme is a mixture of high- and intermediate-spin cytochrome a_3, whereas the a_3 center in the slow form is homogeneously high spin. This is consistent with optical absorbance data from Papadopoulos et al. (1991) and Gullo et al. (1993) by which the rapid conformer was shown to be a mixture of electronic states with estimated center positions at 430 and 414 nm. Alkaline conditions stabilize both the 430 and rapid states.

Formate has also been used to probe the binuclear core, but, unlike cyanide and hydrogen peroxide, this ligand does not simply "report" the relative amounts of rapid and slow forms that are present in a solution of enzyme. Formate is unusual in that, at pH > 8, it induces effects very similar to those observed following an acid jump in the absence of formate, including rapid to slow and 430 to 414 conversions (Schoonover & Palmer, 1991; Moody et al., 1991; Gullo et al., 1993). Formate is presumed by some investigators to insert into the bridging position (which may then be probed by cyanide or hydrogen peroxide); it is this bridged adduct that is thought to be the slow conformer. The similar change induced by an acid jump has implicated a possible role for a highly conserved glutamate residue in putative transmembrane helix VI of the catalytic core subunit (Brown et al., 1993; Cooper et al., 1993). Some controversy exists as to whether the carboxylate insertion is also the direct cause of the 430 to 414 transition or whether a separate structural event accounts for the optical change (Gullo et al., 1993). Some of this uncertainty stems from the difficulty in quantifying the 430 and 414 states due to possible changes in absorptivities

† This investigation was supported by the American Heart Association, Illinois Affiliate Grants C-01 and GS-07.

* Author to whom correspondence should be addressed.

® Abstract published in *Advance ACS Abstracts,* June 15, 1994.

0006-2960/94/0433-8058$04.50/0

under different experiment conditions. Quantitation of the rapid and slow states, based on the use of reporter probes or the amplitude of $g' = 12$, is also subject to complications.

One of the objectives of the current study is to resolve this uncertainty in quantitation and to address critically whether the rapid/slow and 430/414 conformers arise from the same or different structural events. To this end, we have re-examined the binding of formate at pH 8.8, where only rapid conformer is present. Numerical simulation of the kinetic data provides strong support for a rapid equilibrium mixture of 430 and 414 states at the time of the formate addition. We propose that formate reversibly reacts with each of these states to give a kinetic intermediate, denoted 414·L, in which $HCOO^-$ is bound at $Cu_B(II)$. At longer times, a kinetically reversible 414·L → 414′·L conversion occurs, which is interpreted to reflect insertion of $HCOO^-$ into the bridging position to give the slow conformer.

EXPERIMENTAL PROCEDURES

Enzyme Purification and Characterization. The rapid form of cytochrome *c* oxidase was isolated from bovine heart according to the method of Papadopoulos et al. (1991). The final enzyme precipitate was collected by centrifugation, dissolved in 50 mM CHES·KOH/0.1% *n*-dodecyl β-D-maltoside, pH 8.8 at 20 °C, and stored at >500 μM heme *a* (cytochromes $a + a_3$) in liquid nitrogen until use. The heme *a* concentration was quantified according to the method of Papadopoulos et al. (1991). A 5.0 μM heme *a* solution at pH 8.8, 20 °C, showed rigorous one-exponential binding of cyanide (see Figure 3A). All cyanide and formate binding experiments were performed in high ionic strength buffer at pH 8.8, 20 °C.

Preparation of Stock Solutions. A solution of potassium formate (Sigma) was prepared in 50 mM CHES and adjusted to pH 8.8 with KOH at 20 °C. An identically weighed sample, prepared in water, was titrated to the equivalence point with 0.24 M HCl to determine the actual concentration of formate in the CHES buffer. Standardized stocks of 0.96–0.98 or 0.096–0.098 M were used for the binding experiments.

Sodium cyanide (Sigma) was prepared in water and slowly adjusted to pH 8.8, on ice with stirring, usng 6 N HCl. The colorless stock (no oxidative degradation) was assumed to be 4 M, by calculation. No correction was made for volatilized HCN.

Instrumentation. All spectra and time scans were collected with a Shimadzu UV-3000 spectrophotometer in double-beam mode. Sample temperature was regulated at 20 °C using a water bath.

Analysis of Kinetic Models. The time profiles of each dependent variable in a given model were generated by solving a system of coupled first-order ordinary differential equations (ODEs). Mechanisms II and III in the present work did not have general analytical solutions and had to be solved numerically. Curve fitting of the data to the ODEs using initial parameter estimates was not possible since some of the kinetic species were not optically resolvable. Simulations were therefore performed using a fixed set of measured or derived parameters. The ODEs were solved simultaneously using Diffeq (MicroMath Scientific Software, Salt Lake City, UT). The selected numerical approach was the Bulirsch–Stoer method. Step size, interval size, and number of output points were selected to optimize resolution, time frame, and graphics display, respectively.

Statistical weighting of data during least-squares minimization is described and referenced in the appropriate figure legends. Relevant equations and all other kinetic procedures are given under Results.

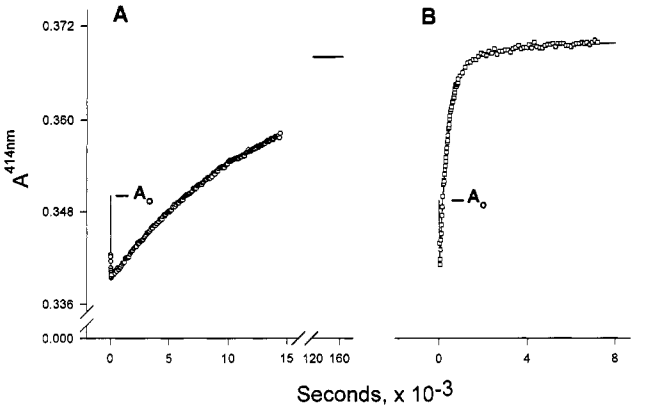

FIGURE 1: Kinetics of formate binding at 1 and 25 mM. (A) Cytochrome *c* oxidase was prepared at 5.7 μM heme *a* in buffer containing 50 mM CHES·KOH, 167 mM K_2SO_4 (μ = 0.5 M), and 0.1% (w/v) *n*-dodecyl β-D-maltoside. The final pH was 8.8 at 20 °C. Potassium formate, buffered at pH 8.8 (see Experimental Procedures), was added to the enzyme solution to give a final concentration of 1 mM. The pH remained stable to within ±0.1 unit. Data collection was initiated at 414 nm after a mixing time of 16 s. Open circles are raw data that have been digitally filtered for clarity of presentation. A two-exponential curve fit of the complete data set (cycle time, 6 s) is shown by the solid line. The extrapolated saturation value is indicated after the *x*-axis break. Observed rate constants were 5.4 × 10^{-2} s^{-1} for the rapid transient and 7.4 × 10^{-5} s^{-1} for the rise phase. The rise was assumed monophasic since data were not collected over the >30 h required for saturation. (B) Same as (A) except 25 mM potassium formate was used and the mixing time was 9 s. The data, shown as open squares, were fit to a three-exponential equation (solid line) with k_{obs} values of 0.2 s^{-1} for the transient, 3.0 × 10^{-3} and 4.4. × 10^{-4} s^{-1} for the rise phases. In (A) and (B) the extrapolated initial absorbance at 414 nm, indicated by A_0, was within 2% of the observed value. Time scans were normalized to 5.0 μM heme *a*.

RESULTS

The Binding of Formate Induces a Transient Red Shift in the Soret Band. The open symbols in Figure 1A,B show the observed absorbance change at 414 nm due to the binding of 1 and 25 mM buffered formate at pH 8.8. The binding reaction was pseudo first order in both cases ($[HCOO^-] \gg$ [heme *a*]). The overlaid solid traces represent multiexponential fits to the open symbols, extrapolated to zero and infinite times. At 1 mM formate (Figure 1A) there was a transient decrease in A^{414} followed by an increase that was monophasic over the measured time course. The initial decrease was not a dilution artifact since the data were collected after the formate addition. The decrease implies a transient red shift in the Soret maximum, followed by a blue shift.

The transient was also observed at 25 mM formate (Figure 1B) but was more difficult to measure by a conventional mixing assay since the subsequent absorbance increase was much faster than that observed at 1 mM. At the higher concentration, the observed increase, measured to saturation, was biphasic, with the slower phase accounting for 12% of the total rise amplitude.

Formate Induces Changes in the Binuclear Core That Are Similar to Those Induced by an Acid Jump. The effect of 10 mM formate on the Soret absorbance band is shown in Figure 2. The dashed spectrum is the pH 8.8 control (minus formate), and the solid spectra show the apparent blue shift induced by the addition of buffered formate. (The absorbance change at 414 nm was used to obtain the kinetic data in Figure

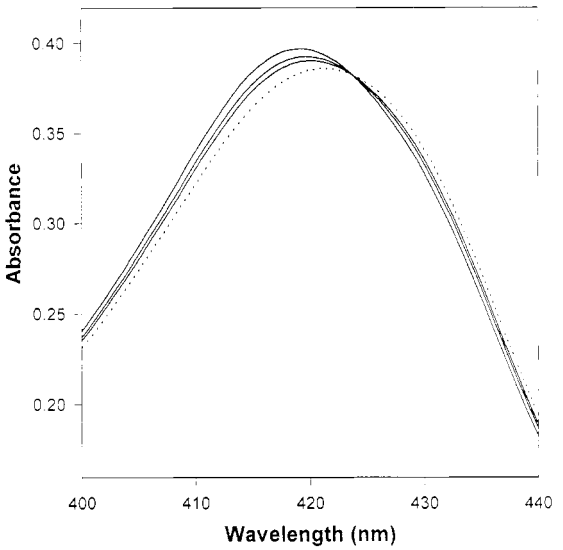

FIGURE 2: Effect of formate binding on the Soret absorbance. A 5.0 μM heme *a* solution was prepared at pH 8.8 as described in Figure 1. (Dashed trace) Control spectrum after 15 min at 20 °C. (Solid traces) Spectra 10, 20, and 40 min following addition of 10 mM buffered formate at pH 8.8, as in Figure 1.

1.) The Soret band was initially at 423.4 nm and, after equilibration with 10 mM formate, had shifted to 419.2 nm with an isosbestic wavelength at 421.2 nm, essentially in agreement with the findings of Schoonover and Palmer (1991). The solid spectra in Figure 2 were recorded over a 40-min period. The k_{obs} value for the slowest phase of the 10 mM formate binding reaction was found by curve fitting in a separate kinetic assay to be 9.0×10^{-4} s^{-1}. After 40 min, this phase was 88% complete. The occurrence of an isosbestic point in Figure 2 indicates that the biphasic increase at 414 nm was not the result of electronic differences in cytochrome a_3 structure. Whether rapid λ scans of the transient would show the same λ_{iso} was not addressed.

The spectra in Figure 2 may also be compared with those obtained after an acid jump [Figure 2B in Papadopoulos et al. (1991)]. Shape, amplitude, and position of λ_{iso} were similar, suggesting that the same 430 → 414 transition in cytochrome a_3 is induced by formate or an acid jump. This optical transition will be assumed in the kinetic models that are discussed below.

In addition to an apparent blue shift in the Soret band, an acid jump induces a rapid to slow transition within the binuclear core that may be detected by measuring the binding kinetics of cyanide or hydrogen peroxide (Baker et al., 1987; Moody et al. 1991; Weng & Baker, 1991). Addition of buffered formate at pH 8.8 also induces the rapid to slow conversion (Moody et al., 1991; Schoonover & Palmer, 1991), as shown in Figure 3. The cyanide binding reaction in the absence of formate (open squares, trace A) was fit rigorously by a single exponential (solid line). The k_{obs} was 0.011 s^{-1} at 25 mM CN^-.

The open circles in trace B show the effect on cyanide binding of pre-equilibrating the same sample with 10 mM formate. The initial absorbance in this case was lower than that of the control since the Soret band was more blue-shifted due to bound formate. Essentially quantitative loss of the rapid conformer was observed. The best fit to the cyanide binding profile, only part of which is shown in trace B, required three exponentials. The fastest phase ($k_{obs} \approx 6 \times 10^{-3}$ s^{-1} at 25 mM CN^-) accounted for <4% of the total, extrapolated absorbance change and the remaining phases had k_{obs} values of 2.2×10^{-4} and 4.9×10^{-5} s^{-1}.

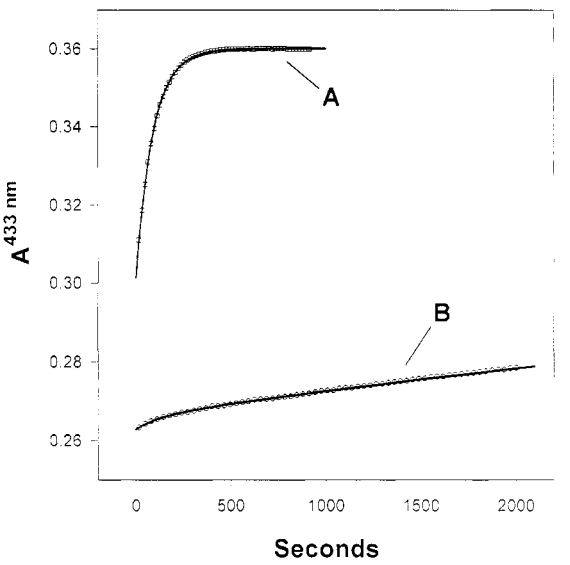

FIGURE 3: Effect of formate preincubation on the cyanide binding reaction. (A) A 5.0 μM heme *a* solution was prepared at pH 8.8, as in Figure 1, and incubated for 15 min at 20 °C (λ_{max} = 423.6 nm). Sodium cyanide was added from a 4 M stock (Experimental Procedures) to a final concentration of 25 mM. The absorbance increase at 433 nm (the λ of maximal change) was measured for 1 h using a 2-s cycle time. Raw data are shown by open squares (truncated to 15 min), and the solid line represents a one-exponential curve fit extrapolated to zero time (k_{obs} = 0.011 s^{-1}). (B) Same as (A) except the enzyme solution was equilibrated with 10 mM potassium formate for 4 h at 20 °C prior to the addition of 25 mM CN^-. The initial absorbance of this sample was lower than that in (A) due to the blue shift induced by formate binding (λ_{max} = 419.8 nm). Data collection occurred over 6 h using a 6-s cycle time. Raw data are indicated by open circles (truncated to 33 min). The solid line is part of a three-exponential fit to the entire 4-h data set, with k_{obs} (percent of total amplitude) values of 6.3×10^{-3} (4%), 2.3×10^{-4} (21%), and 4.9×10^{-5} s^{-1} (75%).

Dependence of k_{obs} on Formate Concentration Suggests Two Possible Kinetic Models. A valid kinetic model for the formate binding reaction must explain (a) the transient decrease at A^{414}, (b) the biphasic increase despite λ_{iso}, and (c) the nearly quantitative rapid to slow transition detected by cyanide. As a first step toward deriving a model, we examined the dependence of the biphasic increase on the concentration of formate. Figure 4 summarizes mean k_{obs} values for five preparations of enzyme at ≥10 mM formate. The open and solid circles refer to the rapid and slow phases, respectively, that were associated with the absorbance increase at 414 nm (text, Figure 1B). Below 10 mM formate the two phases became convergent and showed apparent monophasic behavior (Figure 1A). At ≥10 mM, the data were resolved into two linear regions using weighted regression. The faster phase was clearly dependent on formate, while the weighted fit of the slower phase showed only weak dependence. Although weighting is an accepted remedy for unequal variances in the fitted data (Mannervik, 1983), the amplitude of the standard error bars suggested that the slower phase may, in fact, be zero order-dependent in formate. Two mechanisms (I and II) were therefore consistent with the data in Figure 4:

$$430 + L \underset{k_{-1}}{\overset{k_1}{\rightleftharpoons}} 414 \cdot L \qquad 430 + L \underset{k_{-1}}{\overset{k_1}{\rightleftharpoons}} 414 \cdot L$$

$$430' + L \underset{k_{-2}}{\overset{k_2}{\rightleftharpoons}} 414' \cdot L \qquad 414 \cdot L \underset{k_{-2}}{\overset{k_2}{\rightleftharpoons}} 414' \cdot L$$

I II

In these models, L = HCOOH + $HCOO^-$. The 430 and 430′

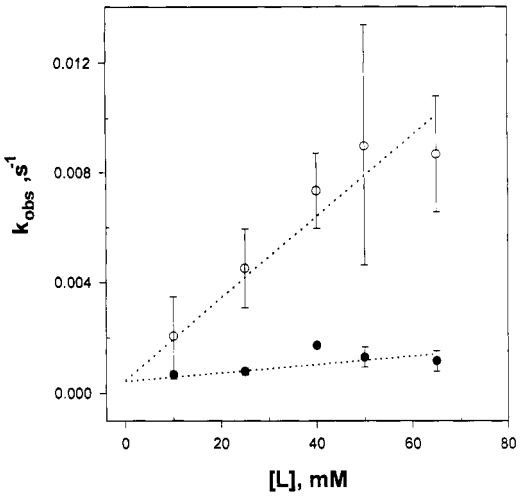

FIGURE 4: Dependence of k_{obs} on formate concentration. Time scans at 10–65 mM formate were obtained as in Figure 1A,B. Each time scan was fit to a two-exponential equation to extract k_{obs} values for the biphasic increase at 414 nm (text, Figure 1B). The transient decrease was not routinely included in these curve fits since it had negligible effect on k_{obs} values for the rapid and slow rise phases. Mean k_{obs} values and standard error bars are shown for five enzyme preparations. Dashed lines represent linear regressions to the means. Since the data showed unequal variances, each mean k_{obs} was weighted as $1/(SE)$.[2] An alternative scheme in which each observed value was weighted as $1/(k_{obs})^2$ (Mannervik, 1983) gave similar results. Slopes and *y*-intercepts of regression lines and their interpretation are given in the text. "[L]" in the *x*-axis label refers to [HCOOH] + [$HCOO^-$].

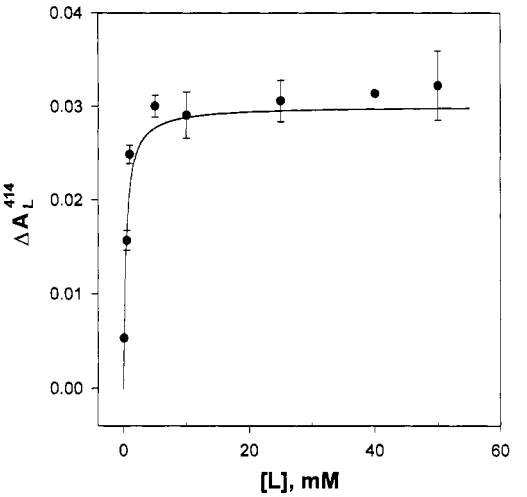

FIGURE 5: Determination of K_D^{app} for the formate binding reaction. The binding reaction at 0.1–50 mM formate was measured as in Figures 1 and 2. Wavelength scans were used to monitor retention of λ_{iso} (Figure 2) and to obtain equilibration data at ≤1 mM formate. The term ΔA_L^{414} is the *net* change in absorbance at 414 nm (footnote 1) due to equilibration with ligand, L. It was correlated with the extent of the blue shift in λ_{max}. Mean values and standard error bars represent data obtained on three to six enzyme preparations. The solid line is a rectangular hyperbolic fit (see text) of the means using the weighting scheme described in Figure 4.

states (mechanism I) are assumed electronically identical, as are the 414·L and 414′·L states (mechanisms I and II). This constraint is required by the isosbestic wavelength in Figure 2. The prime indicates a structural alteration within the catalytic core that causes slower binding of L. Both models assume cytochrome a_3 to be entirely in the 430 (or 430 + 430′) state at the time of formate addition. This will become relevant in later sections.

Equilibrium Analysis of the Formate Binding Reaction Is Consistent with Mechanism II. Measurement of the apparent equilibrium dissociation constant, K_D^{app}, for the formate binding reaction can, in principle, distinguish mechanisms I and II. A value for K_D^{app} was determined from the dependence of the equilibrated absorbance change at 414 nm, ΔA_L^{414}, on the concentration of formate (L).[1] The results of these measurements, shown in Figure 5 for 0.1–50 mM formate, were fit to

$$\Delta A_L^{414} = \Delta A_\infty [L]/(K_D^{app} + [L]) \quad (1)$$

The K_D^{app}, defined as the concentration of L that gives half-maximal saturation, was 0.3 mM at pH 8.8. (The derivation of eq 1, which is of Michaelis–Menten form, assumes a single binding site for L). The measured value of K_D^{app} was not consistent with mechanism I since, for the net equilibrium reaction

$$(430 + 430') + L \rightleftharpoons (414 + 414')\cdot L$$

the expression for K_D^{app} is given by

$$K_D^{app} = \frac{K_{D1}}{1 + (1/\alpha)} + \frac{K_{D2}}{1 + \alpha} \quad (2)$$

where $\alpha = [414\cdot L]/[414'\cdot L]$ and K_{D1} and K_{D2} are the equilibrium dissociation constants for the rapid and slow binding steps in mechanism I, respectively. Given boundary conditions of $\alpha \ll 1$ and $\alpha \gg 1$, eq 2 predicts $K_{D1} \leq K_D^{app} \leq K_{D2}$. If we assume for the moment that mechanism I is valid, then K_{D1} and K_{D2} may be calculated from the weighted linear regressions in Figure 4 (dashed lines). For mechanism I the k_{obs} for each phase is given by $k_i[L] + k_{-i}$, where $i = 1$ or 2 corresponding to the first or second step of the mechanism. K_{Di} is then calculated as k_{-i}/k_i, which gives values of 3 mM for K_{D1} and 28 mM for K_{D2}. The K_D^{app} of 0.3 mM (Figure 5) is not within these limiting values. Replacement of 430′ with 414·L in mechanism I to give a coupled system does not alter the constraint that $K_{D1} \leq K_D^{app} \leq K_{D2}$. Hence, this variation of mechanism I is also excluded.

The K_D^{app} for mechanism II is given by

$$K_D^{app} = K_{D1}/[1 + (1/\alpha)] \quad (3)$$

where α is defined as in eq 2. In the general case, eq 3 predicts $K_D^{app} \leq K_{D1}$, consistent with the measured K_D^{app} of 0.3 mM.

In mechanism II, the slower phase does not depend on the concentration of formate and $k_{obs} = k_2 + k_{-2}$. Assuming a zero slope through the solid circles in Figure 4 gave an approximate value for k_{obs} of 1.0×10^{-3} s^{-1}. The k_{-2}/k_2 ratio ($=\alpha$) was calculated from eq 3 since K_D^{app} and K_{D1} were known (0.3 and 3.0 mM, respectively). A ratio of ≈0.1 indicated that the equilibrium favored the 414′·L state. Separate values for k_2 and k_{-2} were then calculated from $k_2 + k_{-2}$ and k_{-2}/k_2. These were 9.1×10^{-4} and 9.0×10^{-5} s^{-1}, respectively. In the uncoupled limit, the observed rate constant for the fast step of mechanism II is given by $k_{obs} = k_1[L] + k_{-1}$. From the

[1] At any concentration L, the total absorbance change at 414 nm is given by

$$\Delta A_L^{414} = \Delta A_{transient}^{414} + \Delta A_{rapid}^{414} + \Delta A_{slow}^{414}$$

where the transient subscript refers to the initial decrease at 414 nm and the rapid and slow subscripts refer to the biphasic rise to saturation (Figure 1B). At low concentrations of formate (Figure 1A), the rapid and slow terms are not resolvable. By convention, the transient term is negative and the rapid and slow terms are positive. The equilibrium data in Figure 5 for the total absorbance change, ΔA_L^{414}, are plotted using this convention.

slope and y-intercept data in Figure 4, $k_1 = 0.15\ M^{-1}\cdot s^{-1}$ and $k_{-1} = 4.7 \times 10^{-4}\ s^{-1}$.

Effect of a Mixture of 430- and 414-nm States at the Time of Formate Addition: Extension of Mechanism II. Several investigators have provided evidence that cytochrome a_3 at pH >8 is optically and magnetically heterogeneous in the absence of added ligands (Papadopoulos et al., 1991; Moody et al., 1991; Gullo et al., 1993; Day et al., 1933). In particular, Papadopoulos et al. (1991) found that cytochrome a_3 in rapid enzyme was an equilibrium mixture of two electronic states with estimated center positions at 430 and 414 nm. To quantify the fraction of 414-nm centers, Gullo et al. (1993) suggested that $f_{414} = (427 - \lambda_{max})/11$, where λ_{max} is the observed ($a + a_3$) Soret band maximum. At pH 8.8, λ_{max} is 423 nm (dashed line, Figure 2) corresponding to an f_{414} of 0.4. Mechanism II assumed that cytochrome a_3 was entirely in the 430 state. Mechanism III extends that model by including a 430/414 mixture:

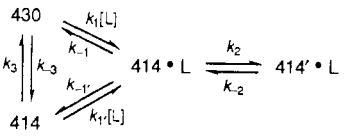

III

The 414 state is separate from either the 414·L or 414′·L state since it is observed in the absence of formate (L). The k_1[L] term is the pseudo-first-order rate constant for the formate-dependent conversion of 430 to 414·L, and a 414 ⇌ 414·L step is postulated with a pseudo-first-order rate constant of $k_{1'}$[L] since there is no reason *a priori* that formate should react only with the 430 state.

Mechanism III does not change the kinetic or equilibrium analysis described above for Figures 4 and 5 if the 430 ⇌ 414 step is in rapid equilibrium. The rapid equilibrium assumption allows d[414·L]/dt to be expressed as $(k_1 f_{430} + k_{1'} f_{414})$[L]·([430] + [414]). The result is that the slope and y-intercept of the open circle fit in Figure 4 give apparent, rather than true, values for the rate constants, with k_1^{app} (the slope) = $k_1 f_{430} + k_{1'} f_{414}$ and k_{-1}^{app} (the y-intercept) = $k_{-1} + k_{-1'}$. It follows that the equilibrium dissociation constant for the 414·L state is $K_{D1}^{app} = k_{-1}^{app}/k_1^{app}$ and that $K_D^{app} \leq K_{D1}^{app}$.[2]

Numerical Simulation of Mechanism III Provides Evidence for a Rapid Equilibrium Mixture of 430 and 414 States. A simulaton of mechanism II, in which all of the a_3 centers were initially assigned to the 430 state, was unable to account for the transient red shifts shown in Figure 1A,B. Only a net increase in 414·L + 414′·L resulted upon addition of L at ≥1 mM. In contrast, a simulation of mechanism III[3] showed transients of correct amplitude, sign, and rate over the experimental range of [L], but only if the initial mixture of 430 and 414 states was assumed to be in rapid equilibrium. To achieve this, the steps for interconverting the 430 and 414 forms were set faster than those for binding L (i.e., $k_{-3} \gg k_1$[L] and $k_3 \gg k_{1'}$[L]).

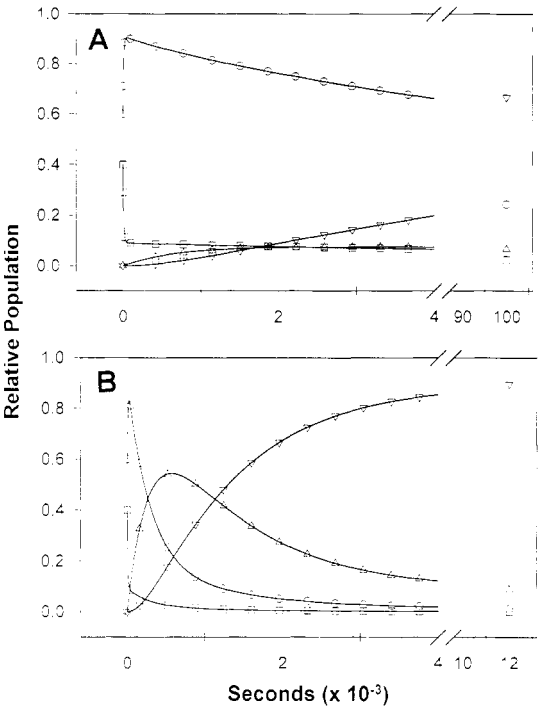

FIGURE 6: Numerical simulation of mechanism III. The numerical approach to simulation is described under Experimental Procedures. The simulation of mechanism III included nine parameters: eight rate constants and [L], where [L] = [HCOOH] + [HCOO⁻]. (A) [L] = 1 mM. (B) [L] = 25 mM. The time profiles of each variable are shown by solid lines overlaid with different symbols. The symbols do not represent actual data points but are simply used to distinguish each profile: (○) 430; (□) 414; (△) 414·L; (▽) 414′·L. The points after the x-axis break represent extrapolated saturation values. Numerical values for the rate constants used in (A) and (B) were derived by the following procedures: As a starting point, the $k_1/k_{1'}$ ratio was assumed to be 5 (see text). From Figure 4, $k_1 + k_{1'} = 0.10\ M^{-1}\cdot s^{-1}$ so that $k_1 = 0.125\ M^{-1}\cdot s^{-1}$ and $k_{1'} = 0.025\ M^{-1}\cdot s^{-1}$. Values for k_3 and k_{-3} (0.10 and 0.01 s^{-1}, respectively) were estimated using the approach outlined in the text. Values for k_{-1} and $k_{-1'}$ were deduced from K_{D1} (footnote 2), and $k_{-1} + k_{-1'} = 4.7 \times 10^{-4}\ s^{-1}$ (Figure 4). K_{D1} was estimated to be 2.7 mM from $K_{D1}^{app}/(K + 1)$, where K_{D1}^{app} = 3.0 mM (Figures 4 and 5), and K (defined as k_{-3}/k_3) = 0.10. Since $K_{D1} = k_{-1}/k_1$, then $k_{-1} = 3.4 \times 10^{-4}\ s^{-1}$ and $k_{-1'} = 1.3 \times 10^{-4}\ s^{-1}$. The two remaining parameters, k_2 and k_{-2}, were measured according to procedures given in the text. They were 9.1×10^{-4} and $9.0 \times 10^{-5}\ s^{-1}$, respectively.

Figure 6 shows the results of a simulation that gave an adequate fit of the data. (An overlay with the actual kinetic data from Figure 1A,B will be shown in Figure 7A,B.) In Figure 6A,B the fraction of each dependent variable (430, 414, 414·L, and 414′·L) is plotted against time at 1 mM formate (A) and 25 mM formate (B). The relevant traces that model the transient behavior in Figure 1A,B are shown by the circles (430) and squares (414). As discussed above, the initial conditions were 0.6 and 0.4 for f_{430} and f_{414}, respectively. The rapid equilibrium condition was applied to the simulation by selecting appropriate values for k_3 and k_{-3}. In particular, a k_3/k_3 ratio >1 was selected to favor the 430 state so that there would be a transient increase in this state (circles) in response

[2] The observed equilibrium reaction for mechanism III is

$$(430 + 414) + L \rightleftharpoons (414 + 414')\cdot L$$

The following definitions

$$K_{D1} = [430][L]/[414\cdot L] \qquad \alpha = [414\cdot L]/[414'\cdot L]$$

lead to eq 4 for the apparent equilibrium dissociation constant

$$K_D^{app} = K_{D1}^{app}/[1 + (1/\alpha)] \qquad (4)$$

where $K_{D1}^{app} = K_{D1}(K + 1)$ and $K = [414]/[430]$. Equation 4 is of the same form as eq 3.

[3] A coupled equilibrium system of the type $A_1 \rightleftharpoons A_2 \rightleftharpoons A_3$ does not have a general analytical solution. In the pseudo-first-order limit, this three-state system is kinetically identical to mechanism II and to mechanism III if the rapid equilibrium assumption is made for the 430 and 414 states. A theoretical analysis of this three-state system can be found in Rodiguin and Rodiguina (1964) for the initial conditions $[A_1]_0 = [A_1]$, $[A_2]_0 = 0$, and $[A_3]_0 = 0$.

to L and, consequently, a transient decrease in 414 (squares). This ratio, which was set to 10 in Figure 6, controlled the amplitude and sign of the 430 and 414 transients as well as the range of [L] over which the transient was observed. For example, a ratio of 2.5 led to a transient decrease in 414 at 1 mM L but not at 25 mM. When the ratio was further decreased to 1.0, f_{414} *increased* rapidly to 0.5 and f_{430} decreased rapidly to 0.5. The sum of k_3 and k_{-3} controlled the rate of the transients and was optimized to give rates similar to those shown in Figure 1. The values of k_3 and k_{-3} that gave satisfactory results were 0.1 and 0.01 s^{-1}, respectively.

The remaining boundary conditions in the simulation were established from the experimental results in Figures 4 and 5. The measured k_1^{app} gave $k_1 f_{430} + k_1 f_{414} = 0.15$ $M^{-1}\cdot s^{-1}$ with $f_{430} = 0.6$ and $f_{414} = 0.4$. Similarly, the k_{-1}^{app} fixed $k_{-1} + k_{-1'}$ at 4.7×10^{-4} s^{-1}. Separate numeric values for k_2 and k_{-2} were also fixed by experiment. Given these constraints, assumptions were then made about the actual numeric values of k_1, $k_{1'}$, k_{-1}, and $k_{-1'}$. For example, the simulations assumed $k_1/k_{1'} = 5$ (i.e., that L reacts with the 430 state at a faster rate than with the 414 state), from which values for k_{-1} and $k_{-1'}$ follow (legend, Figure 6). Using these constraints, the simulation gave a saturation value of $f_{414'\cdot L} = 0.7$ at 1 mM L, in approximate agreement with the equilibrium measurements in Figure 5. (At equilibrium the total 414 pool is $\approx f_{414'\cdot L}$.) A $k_1/k_{1'} = 0.2$ was also examined (with k_{-1} and $k_{-1'}$ adjusted appropriately; legend, Figure 6), but this gave $f_{414'\cdot L} = 0.4$, a value we considered too low when compared with observation.

Uncertainties in k_1, $k_{1'}$, k_{-1}, and $k_{-1'}$ did not affect the amplitude or rate of the transient red shift. This follows from the rapid equilibrium constraint where $k_3 \gg k_1[L]$ (0.1 s^{-1} compared with 3.1×10^{-3} s^{-1} at 25 mM L) and $k_{-3} \gg k_{1'}[L]$ (0.01 s^{-1} compared with 6.3×10^{-4} s^{-1} at 25 mM L).

The saturation values for each kinetic state are also shown by their respective symbols in Figure 6A,B. As stated above, a valid kinetic model must explain several observations, including the nearly quantitative conversion to the slow conformer at ≥10 mM formate (Figure 3). Figure 6B (25 mM formate) shows nearly quantitative conversion to the 414'·L state. Associated with this was a complete loss of 430 and 414 states. Gullo et al. (1993) have argued that a mixture of these states does not prevent 100% rapid binding of cyanide. We will propose under Discussion that it is the 414'·L state that corresponds to the slow conformer that is detected by cyanide or hydrogen peroxide.

Mechanism III Provides a Satisfactory Fit of the Formate Binding Data at 1 and 25 mM. The change in 414-nm absorbance that is observed upon addition of formate represents a change in the *total* 414 pool. Optical absorbance scans cannot resolve the 414, 414·L, and 414'·L states due to the occurrence of an isosbestic wavelength (Figure 2). The multiphasic binding of formate (Figure 1) must therefore result from a multistep mechanism involving only two electronic states (i.e., mechanism III). As a further test of mechanism III, we summed the 414, 414·L, and 414'·L traces in Figure 6A,B and overlaid the result on the time profiles in Figure 1A,B. Since absorptivities were not known for the separate species, the summation was normalized to give the same ΔA_L^{414} as the data. Figure 7 shows the result. The open circles represent the normalized simulation, and the solid traces are the kinetic data at 1 mM formate (A) and 25 mM formate (B). The insets show expanded views of the transient change. The rise portion of the 1 mM case was rigorously monophasic (see text, Figure 1A), but it showed systematic deviations from the raw data that caused an underestimation of the

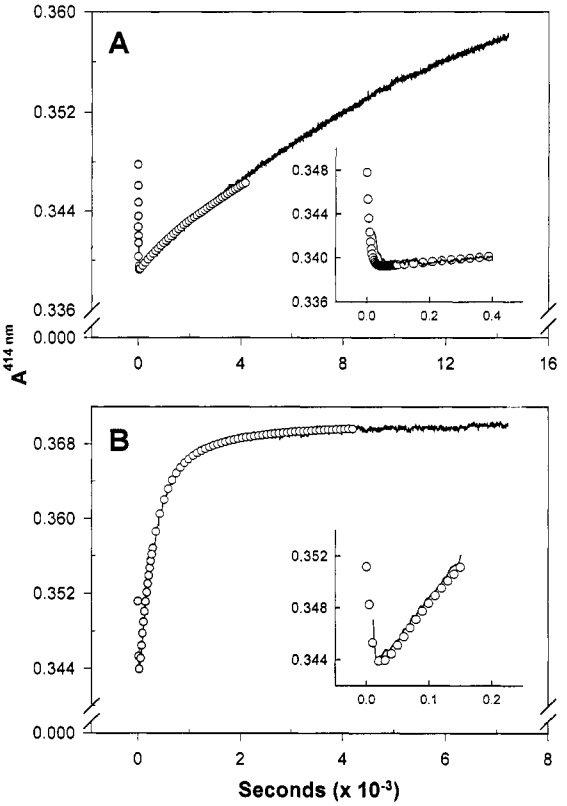

FIGURE 7: Comparison of simulation with actual binding data. (A) The simulated time profiles for 414, 414·L, and 414'·L at 1 mM L (Figure 6A) were added together to give the time dependence of the total 414 pool (open circles). Since absorptivities for each species were unknown, the result was divided by an appropriate scaling factor to optimize comparison with the raw data (solid trace). The inset is an expanded view of the transient time course. (B) Same as (A) except simulation profiles from Figure 6B were used and the concentration of L was 25 mM.

saturation value. To a first approximation, the fit is considered adequate. Further refinements will require experimental determination of k_1 or k_{-1} by analysis of formate binding curves at different initial mixtures of 430 and 414 states. At 25 mM formate (Figure 7B) the simulation replicated, with little systematic deviation, both the transient decrease and biphasic rise that characterized the data. It should be noted that some enzyme preparations showed the transient decrease at 1 mM formate but not at 10 or 25 mM formate. This behavior can be modeled by decreasing the k_3/k_{-3} ratio, as described in the previous section.

DISCUSSION

A kinetic model for the formate binding reaction at pH 8.8 must explain the following observations: (1) a transient absorbance decrease at 414 nm upon addition of formate; (2) a slower, monophasic increase at low concentrations of formate that becomes biphasic at higher concentrations; (3) an apparent two-state optical conversion despite the biphasic increase; (4) the rates and amplitudes of the optical changes induced by formate; and (5) the rapid to slow conversion that is detected by cyanide. Finally, the model should provide a framework for interpreting how the binding of formate at pH 8.8 can mimic the effect of an acid transition.

Mechanism III is shown in the present work to provide a reasonable fit of the optical changes that are induced by formate. The transients, monophasic or biphasic two-state response, and rate and amplitude changes were satisfactorily

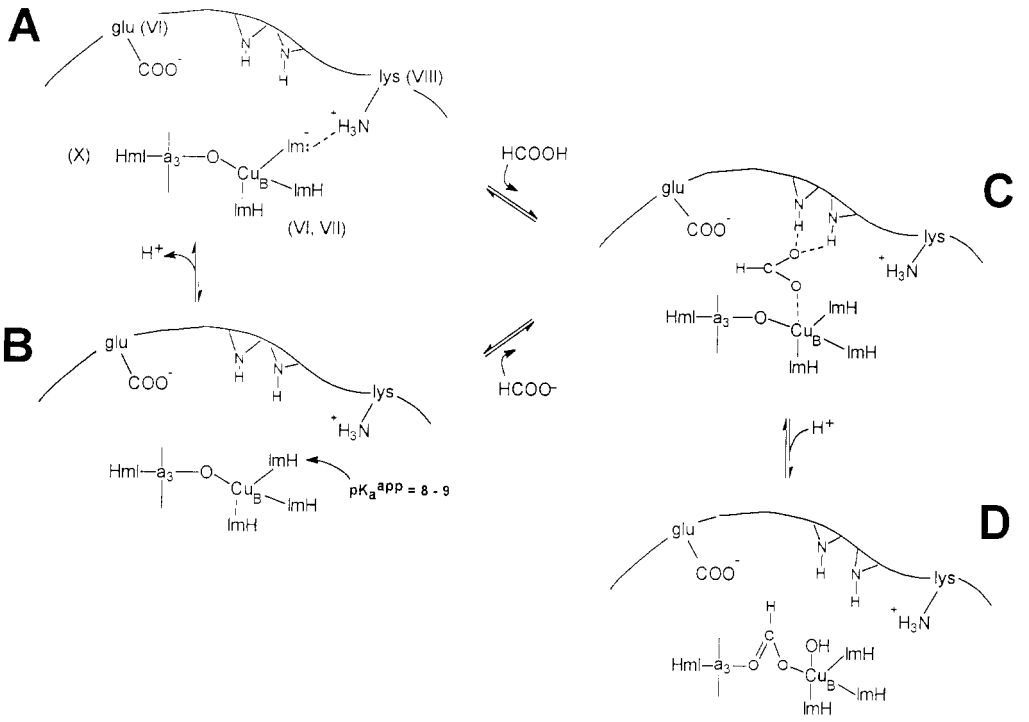

FIGURE 8: Structural model for the binding of formate at pH 8.8. Details of the model are given in the text. Each structural state is identified with a kinetic species in mechanism III: (A) 430, (B) 414, (C) 414·L, and (D) 414′·L. Roman numerals in parentheses (panel A) identify the putative helix (or helices) within subunit I to which the indicated amino acid residues have been assigned.

modeled at both 1 and 25 mM formate (Figure 7). Analysis of these binding data strengthens the argument of Gullo et al. (1993) that cytochrome a_3 is electronically heterogeneous at pH 8.8, despite 100% rapid binding of cyanide. In particular, the transient red shift induced by formate could not be simulated unless a rapid equilibrium mixture of 414 and 430 states was assumed. The red shift required that the equilibrium favor the 430 state (i.e., $k_3/k_{-3} = 10$). A similar model in which $k_3/k_{-3} < 1$ might explain the transient blue shift that is observed upon addition of low concentrations of cyanide to oxidized cytochrome *c* oxidase at pH >8 (Berka et al., 1993).

The 414′·L State May Be the Slow Conformer That Is Detected by Cyanide. There are two ligand-bound states in mechanism III, 414·L and 414′·L, that need to be considered. The possibility that the 414·L state is the slow conformer can be excluded by the simulation in Figure 6B (triangles) since, at 25 mM formate, this species rises and then decays to a fractional equilibrium value of ≈0.1. At equilibrium, this would indicate that there is only 10% conversion to the slow conformer, contrary to the nearly quantitative conversion that is observed (Figure 3).

The other ligand-bound species, 414′·L, is characterized by a small lag, followed by a monotonic increase to a fractional saturation value of ≈0.9 (Figure 6B, inverted triangles). This amplitude is similar to the actual amount of slow conformer that is observed at equilibrium. Furthermore, Gullo et al. (1993) have shown that the k_{obs} for the loss of rapid conformer upon addition of 10 mM formate at pH 8.8 (5.0 μM heme *a*) was about 1.1×10^{-3} s^{-1}. To provide a comparison, the simulation parameters in Figure 6 (see legend) were used to generate a time profile of the 414′·L species at the same ligand concentration. An exponential fit of this profile, using data points after the lag, gave a rate constant of 5.3×10^{-4} s^{-1}, which is only 2-fold slower than the experimentally determined rate of loss for the rapid conformer. An observation that is not explained by this proposal is the irreversibility of the slow conformer by either pH recycling (Baker et al., 1987; Moody et al., 1991) or removal of excess formate by gel filtration (Schoonover & Palmer, 1991). Kinetically, our data indicate that the conversion of 414·L to 414′·L must be reversible since K_D^{app} for the binding of formate (0.3 mM at pH 8.8) is much greater than the total concentration of heme *a* (5 μM).

Structural Model for the Formate Binding Reaction. Following a suggestion by Schoonover and Palmer (1991), Gullo et al. (1993) proposed that the 430 and 414 states arise from imidazolate (Im^-) and imidazole (ImH), respectively, coordinated to Cu_B. Putative structures for these states are shown in Figure 8A,B. A highly conserved lysine residue on transmembrane helix VIII (Gennis, 1992; Babcock & Wikstrom, 1992) is postulated to stabilize the imidazolate charge through ion-paired hydrogen bonding (Figure 8A). This would lower the proton affinity of Im^- and explain the unusually low pK_a^{app} = 8–9 that has been measured for the 414 ⇌ 430 equilibrium (Papadopoulos et al., 1991; Gullo et al., 1993).

The identity of the bridging ligand in the heme–copper oxidases is not clear, but recent papers by Lee and Holm (1993a,b) suggest that a μ-oxo bridge should be considered. Lee and Holm have synthesized an Fe(III)–O–Cu(II) model complex that appears to be a tightly coupled $S = 2$ system with a Soret band transition at 427 nm. Mössbauer parameters were consistent with high-spin Fe(III). This is significant because MCD studies (Baker et al., 1987; Papadopoulos et al., 1991) were inconsistent with a low-spin assignment of the 430 state [cf. Moody et al. (1991)], despite its red-shifted position. The successful synthesis of a high-spin model complex with λ_{max} at 427 nm further argues against a low-spin 430 state. For this reason, a μ-oxo bridge is shown in Figure 8A,B.

Nanthakumar et al. (1993) have synthesized an oxo-bridged (porphyrin)Fe(III)–Cu(II) model complex that can be reversibly protonated at the bridging site, suggesting another possible origin of the 430 ⇌ 414 equilibrium (rather than $-Im^-$ ⇌ –ImH). Additionally, Hosler et al. (1993) have

indicated that a conserved tyrosine residue in helix VI may be a ligand to Cu_B, establishing the possibility that the putative oxo-bridge may be derived from phenoxylate rather than O_2.

Although MCD and model studies are consistent with a high-spin assignment to the 430 state, other data suggest the possibility of intermediate spin. Day et al. (1993) have concluded from magnetization studies that the binuclear core of the rapid conformer is a mixture of $S = 1$ (75%) and $S = 2$ (25%) states. This is similar to the ratio of 430 and 414 forms, respectively, in rapid enzyme at pH 8.8. The $S = 1$ state was proposed, on the basis of magnetization, MCD, and resonance Raman evidence, to result from a strong, antiferromagnetic coupling between intermediate spin a_3^{3+} and Cu_B^{2+}.

A possible structure for 414·L is shown in Figure 8C. The similarity between the effects of formate binding and an acid jump led Gullo et al. (1993) to propose that the 430 → 414·L transition was due to selective diffusion of HCOOH into the binuclear core. Once in the core, the proton transfers from the ligand to Im^-. Direct evidence for this neutral diffusion model is found in some of the peroxidases, as discussed by Gullo et al. (1993). Alternatively, $HCOO^-$ might destabilize the Cu_B–Im^-, shifting the equilibrium toward Cu_B–ImH.

The 414 → 414·L transition may involve uptake of $HCOO^-$, rather than HCOOH, or it may be that the proton from HCOOH is transferred to some other acceptor site within the core. Simulation studies suggest that the preferred binding pathway is 414 → 430 → 414·L (text, Figure 6).

The formate in Figure 8C is shown bound to Cu_B since recent evidence has implicated a kind of "gateway" in which certain ligands entering the catalytic core must first bind to the copper before interacting with a_3 (Lemon et al., 1993). The Cu_B in Figure 8C is pentacoordinate (Cooper et al., 1993), although controversy exists over whether there are two or three histidines bound at the Cu_B site (Calhoun et al., 1993a). The $HCOO^-$ is also shown interacting with NH groups of peptide linkages within the core to provide additional stabilization energy [Meot-Ner (Mautner), 1988].

The formation of 414′·L (Figure 8D) presumably results from insertion of $HCOO^-$ into the bridging position, displacing the μ-oxygen onto Cu_B. A similar formate-bridged structure has been suggested by Brown et al. (1993) and Cooper et al. (1993) to be the origin of the slow conformer, and there is now clear FTIR evidence that cyanide, which is often used to quantify the slow conformer, forms a bridge between the a_3(III) and Cu_B(II) sites (Caughey et al., 1993; Tsubaki & Yoshikawa, 1993). This result is consistent with a model in which the formate bridge must first dissociate before cyanide can bind. In support of this, the pseudo-first-order rate constant for the binding of 25 mM cyanide in enzyme pre-equilibrated with formate is 5.5×10^{-5} s^{-1} (J. Tayh and G. M. Baker, unpublished data), whereas the dissociation rate constant for 414′·L (k_{-2}) is 9.0×10^{-5} s^{-1} (text, Figures 4 and 5). Thus, the binding rate of cyanide is similar to the rate at which formate dissociates.

Double-bridged structures should also be considered as possible models for the slow conformer. Recent crystal structures for bacterial xylose isomerase show the carboxylate of a glutamate residue bridging two Mg(II) ions. When the substrate is bound, the carboxylate bridge remains intact but an oxygen from the open chain sugar inserts between the two magnesiums to form a second bridge that causes the Mg ions to move 1 Å closer together (Allen et al., 1994; G. Petsko, personal communication). Similar double-bridged structures have also been found in Zn–Zn, Zn–Mg, Mn–Mg, Mn–Mn, and Fe–Fe (G. Petsko, personal communication). This suggests the interesting possibility that formate and a second ligand (derived, for example, from O_2 or tyrosine) may simultaneously bridge the a_3 and Cu_B sites.

Proton Binding and the Effect of an Acid Jump. The transition from 414·L to 414′·L is predicted to involve concerted proton uptake to give, formally, Cu_B(II)–OH^- (Figure 8D). This structure would be consistent with the proposed role of Cu_B in proton translocation (Mitchell, 1987; Babcock & Wikstrom, 1992; Brown et al., 1993). Reduction experiments with dithionite have shown the slow conformer to be heterogeneous, possibly due to OH^-/H_2O exchange at the Cu_B site (Cooper et al., 1993). Whether this type of exchange affects the formate binding reaction is not yet clear, but it might explain the predominantly biphasic reaction with cyanide in enzyme that has quantitatively converted to 414′·L (trace B, Figure 3).

The proton binding steps in mechanism III have not been experimentally identified. Currently, we are examining the pH dependence of the formate binding reaction to identify these steps and to extend the mechanism, if necessary, to explain the reaction over a broad range of pH. No kinetic model is yet available that can explain the dramatic increase in the binding rate of formate as the pH is decreased (Moody et al., 1991; Schoonover & Palmer, 1991).

A conserved glutamate residue on helix VI is included in each of the panels in Figure 8 since Brown et al. (1993) have suggested this residue to be the origin of the rapid to slow conversion that is induced in the absence of formate by an acid jump. Direct evidence for the positioning of helix VI in the distal pocket of cytochrome a_3 has recently been reported by Calhoun et al. (1993a,b). The current model orients helix VI so that a conserved histidine and tyrosine can interact with the Cu_B site. Given this assumption, the glutamate would be on the opposite side of helix VI and would not be able to interact with the binuclear center. Hosler et al. (1993), however, point out that this part of helix VI may not be α-helical since it is near a conserved G-H-P sequence that is commonly found in protein turns. In work to be presented elsewhere, we show that the proposed carboxylate insertion (414·L ⇌ 414′·L) is modulated by the amount of bound phospholipid, suggesting that a change in protein conformation is involved in this step.

Does the Position of the Soret Band Allow Quantitation of the 430/414$_{total}$ Distribution? Gullo et al. (1993) have used the formula $f_{414} = (427 - \lambda_{max})/11$ to quantify the total amount of 414 present in an enzyme solution in the presence or absence of formate (see Results). On the basis of this approach, Gullo et al. (1993) concluded that 30% of the cytochrome a_3 centers were still at 430 nm ($f_{414} = 0.7$) after equilibration with 10 or 25 mM formate at pH 8.8. The simulation in Figure 6B, however, is not consistent with this formula-based prediction since f_{430} becomes essentially zero at equilibrium (open circles). The discrepancy between formula and simulation suggests that there may not always be a simple linear relationship between λ_{max} and the 430/414$_{total}$ distribution. Such a relationship assumes that $\epsilon^{414} = \epsilon^{414\cdot L} = \epsilon^{414'\cdot L}$, but absorptivities may depend in different ways on pH, the detergent/heme *a* ratio, or whether formate is present. The simulation study, outlined in the present work, may represent the best approach to quantifying the separate kinetic states.

ACKNOWLEDGMENT

We thank Professor James Erman in the Chemistry Department at Northern Illinois University for helpful discussions.

REFERENCES

Allen, K. N., Lavie, A., Glasfeld, A., Tanada, T. N., Gerrity, D. P., Carlson, S. C., Farber, G. K., Petsko, G. A., & Ringe, D. (1994) *Biochemistry 33*, 1488–1494.

Babcock, G. T., & Wikstrom, M. (1992) *Nature 356*, 301–309.

Baker, G. M., Noguchi, M., & Palmer, G. (1987) *J. Biol. Chem. 262*, 595–604.

Berka, V., Vygodina, T., Musatov, A., Nicholls, P., & Konstantinov, A. A. (1993) *FEBS Lett. 315*, 237–241.

Brown, S., Moody, J. A., Mitchell, R., & Rich, P. R. (1993) *FEBS Lett. 316*, 216–223.

Brudvig, G. W., Stevens, T. H., Morse, R. H., & Chan, S. I. (1981) *Biochemistry 20*, 3912–3921.

Brudvig, G. W., Morse, R. H., & Chan, S. I. (1986) *J. Magn. Reson. 67*, 189–201.

Calhoun, M. W., Thomas, J. W., Hill, J. J., Hosler, J. P., Shapleigh, J. P., Tecklenburg, M. M. J., Ferguson-Miller, S., Babcock, G. T., Alben, J. O., & Gennis, R. B. (1993a) *Biochemistry 32*, 10905–10911.

Calhoun, M. W., Lemieux, L. J., Thomas, J. W., Hill, J. J., Goswitz, V. C., Alben, J. O., & Gennis, R. B. (1993b) *Biochemistry 32*, 13254–13261.

Caughey, W. S., Dong, A., Sampath, V., Yoshikawa, S., & Zhao, X.-J. (1993) *J. Bioenerg. Biomembr. 25*, 81–91.

Cooper, C. E., & Salerno, J. C. (1992) *J. Biol. Chem. 267*, 280–285.

Cooper, C. E., Junemann, S., Ioannidis, N., & Wrigglesworth, J. M. (1993) *Biochim. Biophys. Acta 1144*, 149–160.

Day, E. P., Peterson, J., Sendova, M. S., Schoonover, J. R., & Palmer, G. (1993) *Biochemistry 32*, 7855–7860.

Gennis, R. B. (1992) *Biochim. Biophys. Acta 1101*, 184.

Gullo, S. M., Tayh, J. A., Li, J., & Baker, G. M. (1993) *Arch. Biochem. Biophys. 307*, 78–84.

Hosler, J. P., Ferguson-Miller, S., Calhoun, M. W., Thomas, J. W., Hill, J., Lemieux, L., Ma, J., Georgiou, C., Fetter, J., Shapleigh, J., Tecklenburg, M. M. J., Babcock, G. T., & Gennis, R. B. (1993) *J. Bioenerg. Biomembr. 25*, 121–136.

Lee, S. C., & Holm, R. H. (1993a) *J. Am. Chem. Soc. 115*, 5833–5834.

Lee, S. C., & Holm, R. H. (1993b) *J. Am. Chem. Soc. 115*, 11789–11798.

Lemon, D. D., Calhoun, M. W., Gennis, R. B., & Woodruff, W. H. (1993) *Biochemistry 32*, 11953–11956.

Mannervik, B. (1983) in *Contemporary Enzyme Kinetics and Mechanism* (Purich, D. L., Ed.) pp 75–95, Academic Press, New York.

Meot-Ner (Mautner), M. (1988) *J. Am. Chem. Soc. 110*, 3071–3075.

Mitchell, P. (1987) *FEBS Lett. 222*, 235–245.

Moody, A. J., Cooper, C. E., & Rich, P. R. (1991) *Biochim. Biophys. Acta 1059*, 189–207.

Nanthakumar, A., Fox, S., Murthy, N. N., Karlin, K. D., Ravi, N., Huynh, B. H., Orosz, R. D., Day, E. P., Hagen, K. S., & Blackburn, N. J. (1993) *J. Am. Chem. Soc. 115*, 8513–8514.

Palmer, G., Baker, G. M., & Noguchi, M. (1988) *Chem. Scr. 28A*, 41–46.

Papadopoulos, P. G., Walter, S. A., Li, J., & Baker, G. M. (1991) *Biochemistry 30*, 840–850.

Rodiguin, N. M., & Rodiguina, E. N. (1964) in *Consecutive Chemical Reactions: Mathematical Analysis and Development*, Van Nostrand, Princeton, NJ.

Schoonover, J. R., & Palmer, G. (1991) *Biochemistry 30*, 7541–7550.

Tsubaki, M., & Yoshikawa, S. (1993) *Biochemistry 32*, 164–173.

Weng, L. & Baker, G. M. (1991) *Biochemistry 30*, 5727–5733.